THE JOURNAL OF BIOLOGICAL CHEMISTRY VOL. 290, NO. 48, pp. 28857–28868, November 27, 2015
Published in the U.S.A.

A Novel MHC-I Surface Targeted for Binding by the MCMV m06 Immunoevasin Revealed by Solution NMR*

Received for publication, September 3, 2015, and in revised form, October 8, 2015 Published, JBC Papers in Press, October 13, 2015, DOI 10.1074/jbc.M115.689661

Nikolaos G. Sgourakis[‡1,2], **Nathan A. May**[§1], **Lisa F. Boyd**[§], **Jinfa Ying**[‡], **Ad Bax**[‡3], **and David H. Margulies**[§4]

From the [‡]*Laboratory of Chemical Physics, NIDDK, and the* [§]*Molecular Biology Section, Laboratory of Immunology, NIAID, National Institutes of Health, Bethesda, Maryland 20892*

Background: The m06/gp48 protein of MCMV binds to MHC-I proteins, diverting them to lysosomes.
Results: Recombinant m06 binds weakly to H2-L^d MHC-I and tightly to mini-H2-L^d, which provides excellent NMR spectra for mapping the binding site.
Conclusion: The binding site on MHC-I partially overlaps with the β_2m interface.
Significance: Thus, m06 may alter the conformation of β_2m association with MHC-I heavy chain following m06 binding in a viral infection.

As part of its strategy to evade detection by the host immune system, murine cytomegalovirus (MCMV) encodes three proteins that modulate cell surface expression of major histocompatibility complex class I (MHC-I) molecules: the MHC-I homolog m152/gp40 as well as the m02-m16 family members m04/gp34 and m06/gp48. Previous studies of the m04 protein revealed a divergent Ig-like fold that is unique to immunoevasins of the m02-m16 family. Here, we engineer and characterize recombinant m06 and investigate its interactions with full-length and truncated forms of the MHC-I molecule H2-L^d by several techniques. Furthermore, we employ solution NMR to map the interaction footprint of the m06 protein on MHC-I, taking advantage of a truncated H2-L^d, "mini-H2-L^d," consisting of only the $\alpha 1\alpha 2$ platform domain. Mini-H2-L^d refolded *in vitro* with a high affinity peptide yields a molecule that shows outstanding NMR spectral features, permitting complete backbone assignments. These NMR-based studies reveal that m06 binds tightly to a discrete site located under the peptide-binding platform that partially overlaps with the β_2-microglobulin interface on the MHC-I heavy chain, consistent with *in vitro* binding experiments showing significantly reduced complex formation between m06 and β_2-microglobulin-associated MHC-I. Moreover, we carry out NMR relaxation experiments to characterize the picosecond-nanosecond dynamics of the free mini-H2-L^d MHC-I molecule, revealing that the site of interaction is highly ordered. This study provides insight into the mechanism of the interaction of m06 with MHC-I, suggesting a structural manipulation of the target MHC-I molecule at an early stage of the peptide-loading pathway.

The endogenous protein antigen processing and presentation pathway provides the cell with an important surveillance mechanism that protects against invading pathogens. This involves the cell surface display of intracellularly processed protein fragments within the peptide-binding groove of fully assembled MHC-I molecules (including the light chain β_2m) for recognition by CD8$^+$ cytotoxic T cells and NK cells. To counter this host defense, viruses that establish long term latent or persistent infections have evolved intricate strategies to evade the immune response (1). MCMV[5] encodes three proteins that interact with MHC-I to interfere with T cell and NK cell recognition of infected cells: m152/gp40, itself an MHC-I structural homolog, as well as m06/gp48 and m04/gp34, members of the MCMV m02-m16 family (2). The m152 protein is believed to associate transiently with MHC-I molecules and, by an unknown mechanism, arrest MHC-I maturation in the early secretory pathway (3, 4). Although both m04 and m06 bind MHC-I, their association has varying effects; m06 reroutes MHC-I molecules to lysosomes using a dileucine sorting signal encoded in its cytoplasmic tail (5), whereas m04 partially counters the maturation arrest of m152, allowing a fraction of the cell's MHC-I molecules to reach the cell surface (6, 7). Although there are several genetic and functional studies on the combined effects of m04 and m06 interference with MHC-I (7–10), the exact molecular mechanism of their interaction with MHC-I remains unknown, in part due to impediments to the co-crystallization of their complexes.

NMR spectroscopy provides an attractive alternative to crystallography for studying the structure and dynamics of macromolecular assemblies in solution. When isotope-labeled molecules can be recombinantly expressed and purified in milligram quantities, solution NMR is a powerful technique to map the

* This research was supported by the intramural research programs of the NIDDK and NIAID, National Institutes of Health. The authors declare that they have no conflicts of interest with the contents of this article.
[1] Both authors contributed equally to this work.
[2] Present address: Dept. of Chemistry and Biochemistry, University of California Santa Cruz, 1156 High St., Santa Cruz, CA 95064.
[3] To whom correspondence may be addressed: Laboratory of Chemical Physics, NIDDK, National Institutes of Health, Bldg. 5, Rm. 126, 5 Memorial Dr., Bethesda, MD 20892-0520. Tel.: 301-496-2848; Fax: 301-402-0907; E-mail: bax@nih.gov.
[4] To whom correspondence may be addressed: Molecular Biology Section, Laboratory of Immunology, NIAID, National Institutes of Health, Bldg. 10, Rm. 11N311, 10 Center Dr., Bethesda, MD 20892-1892. Tel.: 301-496-6429; Fax: 301-496-0222; E-mail: dhm@nih.gov.
[5] The abbreviations used are: MCMV, mouse cytomegalovirus; TCR, T cell receptor; β_2m, β_2-microglobulin; SPR, surface plasmon resonance; RDC, residual dipolar coupling; PDB, Protein Data Bank.

interaction surfaces, to determine the conformations of bound ligands and complex structures, and to characterize any dynamic and conformational changes upon binding. Previous NMR (11) and x-ray (12) structural studies of the m04 luminal domain concurrently revealed an intricate variant of the Ig-fold that is conserved among members of the m02-m16 immmunoevasin family, including m06, suggesting a conserved mechanism for MHC-I binding. Using high resolution NMR, Varani *et al.* (13) exploited a truncated H2-L^d molecule to map the binding site of the 2C T cell receptor on the peptide·MHC-I complex. First, they engineered mini-H2-L^d, a minimal $\alpha1\alpha2$ platform molecule derived from the murine H2-L^d protein, which lacks the $\alpha3$ domain and does not require the light chain β_2m for refolding *in vitro* (14). Subsequent structural characterization showed that this molecule preserves the binding epitopes for T cell recognition in their native orientation, as indicated by co-crystal structures of several peptide·MHC-I/TCR complexes (15). More recently, solution NMR studies of the 2C/mini-H2-L^d system explored recognition dynamics at the MHC-I/TCR interface (16, 17).

Here we examine the interaction of an additional member of the m02 family, m06, with the mini-H2-L^d construct. We employ bacterially expressed recombinant m06 as well as full-length H2-L^d·β_2m and mini-H2-L^d refolded with a high affinity peptide as probes to characterize these interactions. The ability to make complete backbone assignments of mini-H2-L^d permitted us to characterize its interaction with m06 through a discrete site located under the peptide-binding platform that partially overlaps with the β_2m interface on the MHC-I heavy chain. The identification of this region is consistent with *in vitro* binding experiments showing much weaker complex formation between m06 and β_2m-associated MHC-I. NMR relaxation experiments characterize the picosecond-nanosecond dynamics of the free MHC-I molecule. This study defines an MHC-I binding site for a member of the m02-m16 family and suggests a novel strategy exploited by a viral immunoevasin to bind MHC-I molecules.

Experimental Procedures

Protein Production and Purification—The luminal domain of MCMV m06 was PCR-amplified from the plasmid gp48HA-PPM (originally amplified from Smith strain MCMV Bac DNA), the kind gift of Dr. A. Hudson (18), using primers 5′-TTTTTTCATATGGGAGAATCGCTAATA-3′ and 5′-TTTTTTGGATCCTTACTGGCGGCGGCGGCGTGATGG-3′ and cloned into pET21b. The codon encoding the cysteine at m06 position 47 was mutated to alanine by PCR mutagenesis using primers 5′-ATCGTGGGGGCCAACGTTTCGCGTACCGAG-3′ and 5′-AACGTTGGCCCCCACGATAGGTTCCTC-3′ and verified by DNA sequencing. The luminal domain of m06 was expressed in Rosetta 2 (DE3) *Escherichia coli* as inclusion bodies. Following washing in Tris/EDTA and solubilization in 6 M guanidine HCl, protein was refolded by dilution into refolding buffer (0.4 M arginine HCl, 0.1 M Tris, pH 8, 2 mM EDTA, 5 mM reduced glutathione, 0.5 mM oxidized glutathione) for 4 days at 4 °C; dialyzed against 150 mM NaCl and 25 mM MES, pH 6.5; concentrated with an Amicon stirred cell concentrator using an Ultracel 10-kDa ultrafiltration-regenerated cellulose filter (Millipore); purified by gel filtration on Superdex HR 75 in the same buffer; and maintained at a temperature of 4 °C. The luminal domain of H2-L^d was expressed from a pET3a plasmid as inclusion bodies in BL21 *E. coli* and refolded with peptide YPNVNIHNF ("NIH peptide") (19) and murine or human β_2m, as described for H2-D^d (20). The luminal domain of H2-D^d was also refolded with peptide RGPGRAFVTI ("P18-I10 peptide") and murine β_2m as described (20). Mini-H2-L^d in pET28a (14), the kind gift of Dr. D. Kranz, was expressed as inclusion bodies in BL21 Codon Plus (DE3) RIPL cells and refolded with the NIH peptide or QL9 peptide (sequence QLSPFPFDL (21)). Protein was purified by gel filtration and ion exchange chromatography on mono-Q, showing a single, monodisperse peak in the chromatogram. Isotope-labeled preparations of H2-L^d were made with a similar protocol but instead using ^{13}C-, ^{15}N-, and ^{2}H-substituted M9 minimal media to prepare the inclusion bodies as described for m04 (11).

Surface Plasmon Resonance (SPR)—For the experiments shown, monoclonal antibody 30-5-7S (22), which binds the $\alpha2$ domain of H2-L^d (23), was covalently coupled to a BIAcore T100 CM5 surface by standard NHS-EDC chemistry as described previously (24). Then either full-length H2-L^d refolded with the NIH peptide and either mouse or human β_2m or mini-H2-L^d was captured on the antibody surface, followed by offering m06 to the captured H2-L^d in graded concentrations. In competition experiments, mini-H2-L^d was first captured and then exposed to different concentrations of m06 prior to being offered 1.2 mM murine β_2m. Apparent dissociation rates were calculated using BIAevaluation software. All SPR experiments were performed at 10 °C.

Native Gel Shift Assays—Protein samples were incubated in native gel loading buffer (250 mM Tris, pH 8.8, 10% glycerol) for 30 min at 4 °C. Samples were loaded on 8% polyacrylamide gels at 90 V (constant voltage) at 4 °C for 3.5 h in 25 mM Tris and 190 mM glycine running buffer. Following electrophoresis, proteins were visualized with PageBlue protein staining solution (Thermo Scientific) or transferred to a nitrocellulose membrane for immunoblot analysis.

Immunoblotting—Following native gel electrophoresis, proteins were transferred to a BA-85 nitrocellulose membrane (Schleicher & Schuell, Keene, NH) and probed with 64-3-7 primary antibody (25), followed by an HRP-conjugated goat anti-mouse secondary antibody (Invitrogen). Bands were visualized using Pierce SuperSignal chemiluminescence reagents (Thermo Scientific).

NMR Backbone and Side Chain Assignments, and Backbone Relaxation Rate Measurements—All experiments were recorded at a temperature of 25 °C using 600-, 800-, and 900-MHz cryoprobe-equipped Bruker spectrometers. We used an array of TROSY-based triple-resonance assignment experiments (HNCO, HN(CA)CO, HNCA, and HN(CA)CB), recorded at 600 MHz, supplemented with H(N)NH and (H)NNH three-dimensional NOESY-HSQC data sets, recorded at 800 or 900 MHz. For monomeric mini-H2-L^d samples, we used non-uniform sampling versions of the three-dimensional experiments at 50% levels of sparsity with mixed time ^{15}N (26) and constant time ^{13}C (27) evolution periods when needed

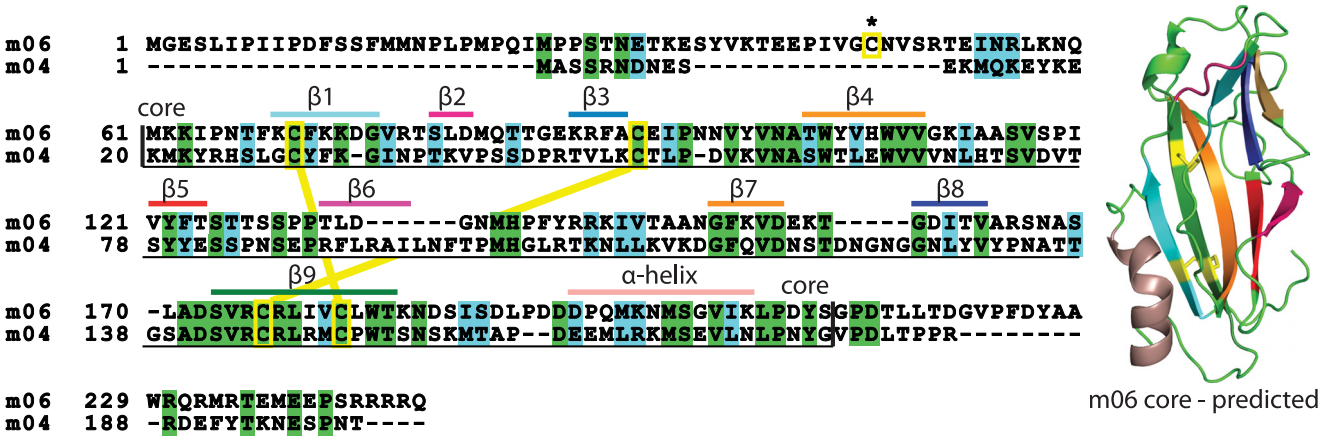

FIGURE 1. **Structural conservation of the endoplasmic reticulum-luminal domains of m04 and m06 MCMV immunoevasins.** The approximate positions of conserved secondary structure elements are highlighted at the *top* of each alignment block (*β1–β9*, *β*-strands). The positions of the two disulfide bonds shared by m04 core and the model of m06 are indicated with *yellow brackets* and *connecting yellow lines*, whereas the position of a free cysteine in m06 is indicated with a *yellow bracket* and an *asterisk*. Sequence alignment was generated using m04 sequence from PDB entry 2MIZ (11), and a homology-based model of m06 was generated with I-TASSER (38), using the first model in the NMR ensemble of m04 as a structural template (PDB entry 2MIZ) (11).

(HNCA and HN(CA)CB). For NMR binding experiments, unlabeled m06 was mixed with either 110 μM full-length (^{13}C/^{15}N/^{2}H-labeled heavy chain with unlabeled human β_2m and peptide) or 100 μM labeled mini-H2-L^d MHC-I at a ~1:1 ratio in matched buffer (50 mM NaCl, 20 mM PIPES, pH 6.4). To assign the bound state of mini-H2-L^d in the 53-kDa MHC-I·m06 complex, we switched to standard (incrementally sampled), non-constant time three-dimensional experiments with optimized INEPT transfer delays and shorter acquisition times in the indirect dimensions (30 ms in ^{15}N, 20 ms in ^{13}CO, and 10/5 ms in $^{13}C_{\alpha/}{}^{13}C_{\beta}$. All resulting spectra were processed with NMRPipe (28) and analyzed with Sparky (29). Resonance assignments have been deposited in the Biological Magnetic Resonance Data Bank under ID 26646.

A full set of R_1, $R_{1\rho}$, and ^{15}N-{^{1}H} NOE relaxation spectra were recorded at 600 MHz and supplemented with R_1 measurements at 900 MHz from a 0.9 mM perdeuterated, amide ^{1}H sample using TROSY readout methods (30). R_2 rates were obtained from rotating frame $R_{1\rho}$ rates (31) measured under a spin-lock field strength of 2 kHz, after correction for the ^{15}N off-resonance, tilted field. Uncertainties in the R_1 and $R_{1\rho}$ measurements were estimated from the spectral noise levels using 21 Monte Carlo simulations, whereas uncertainties in the ^{15}N-{^{1}H} NOE ratios were propagated directly from the noise levels in the reference and attenuated spectra. To assess consistency between R_1 and R_2 rates and the presence of oligomer formation in the sample, we performed simulations of relaxation rates under the full spectral density function formalism using an in-house perl script. To measure backbone amide residual dipolar couplings (RDCs), we prepared a liquid crystalline sample containing 15 mg/ml Pf1 phage in 50 mM NaCl (32). We used the ARTSY method for quantitative measurement of RDCs at 900 MHz (33). The agreement of the experimentally determined RDCs to the x-ray structure of mini-H2-Ld (PDB entry 3TF7) is quantified by the Q-factor, which reports the deviation of the back-calculated RDCs using the crystallographic coordinates relative to a range of RDCs estimated from a randomly distributed set of vectors assuming an alignment tensor of Known D_a and R parameters,

$$Q = \frac{RMS\ (D_{calc} - D_{obs})}{\sqrt{D_a^2\,(4 + 3R^2)/5}} \qquad \text{(Eq. 1)}$$

where D_a and R represent the magnitude and rhombicity of the alignment tensor, and D_{calc} and D_{obs} are the calculated and observed RDCs, respectively. The five parameters of the alignment tensor were determined by best-fitting, using a singular value decomposition process (34), of the experimental RDCs to the x-ray coordinates of mini-H2-Ld in complex with the QL9 peptide (PDB entry 3TF7), yielding $D_a = -15.4$ Hz, and R = 0.29. The fitting process was carried out using custom-built routines within the program Rosetta (35).

Results

Direct Interaction between m06 and H2-L^d MHC-I—Initial preparations of the recombinant full-length luminal domain of m06, excluding the transmembrane and cytosolic domains, were prone to precipitation and interchain disulfide bond formation. From a sequence alignment with the structurally related m04 protein, we identified a putatively free cysteine in m06 at position 47 (Fig. 1). Mutagenesis of Cys-47 to Ala resulted in the significantly more stable m06 protein used in this study. To evaluate the ability of m06 to bind MHC-I molecules, we first performed native gel shift assays, mixing recombinant m06 with different MHC-I constructs. Guided by previously reported co-immunoprecipitation results (5, 36), we probed for binding of the MHC-I allotype H2-L^d to the recombinant m06 (Fig. 2*a*). The MHC-I constructs were refolded *in vitro* from bacterially produced inclusion bodies in the presence of murine β_2m and the high affinity NIH peptide (19, 37). These first assays were consistently negative using different peptide·MHC-I complexes, including H2-D^d and H2-L^d refolded with human β_2m (Fig. 2, *a* and *b*). We then turned to the previously engineered mini-H2-L^d protein that lacks the α3 domain and does not require β_2m for refolding or peptide binding (14). Preliminary screening of mini-H2-L^d for m06 binding by a native gel shift assay revealed the appearance of a new band, migrating more slowly than the mini-H2-L^d construct alone (Fig. 2*c*). To confirm that the new band represented a complex

containing mini-H2-L^d, we subsequently transferred proteins to a membrane and immunoblotted with the 64-3-7 antibody, which detects an epitope on the H2-L^d α1 domain (39) (Fig. 2*d*). Considering that 64-3-7 recognizes a linear epitope present only on MHC-I molecules lacking peptide, we interpret this signal as detecting those H2-L^d molecules that have lost peptide during the process of transfer to the nitrocellulose membrane, following native gel electrophoresis.

To validate further the interaction between m06 and H2-L^d, we performed SPR binding studies, first capturing H2-L^d on a

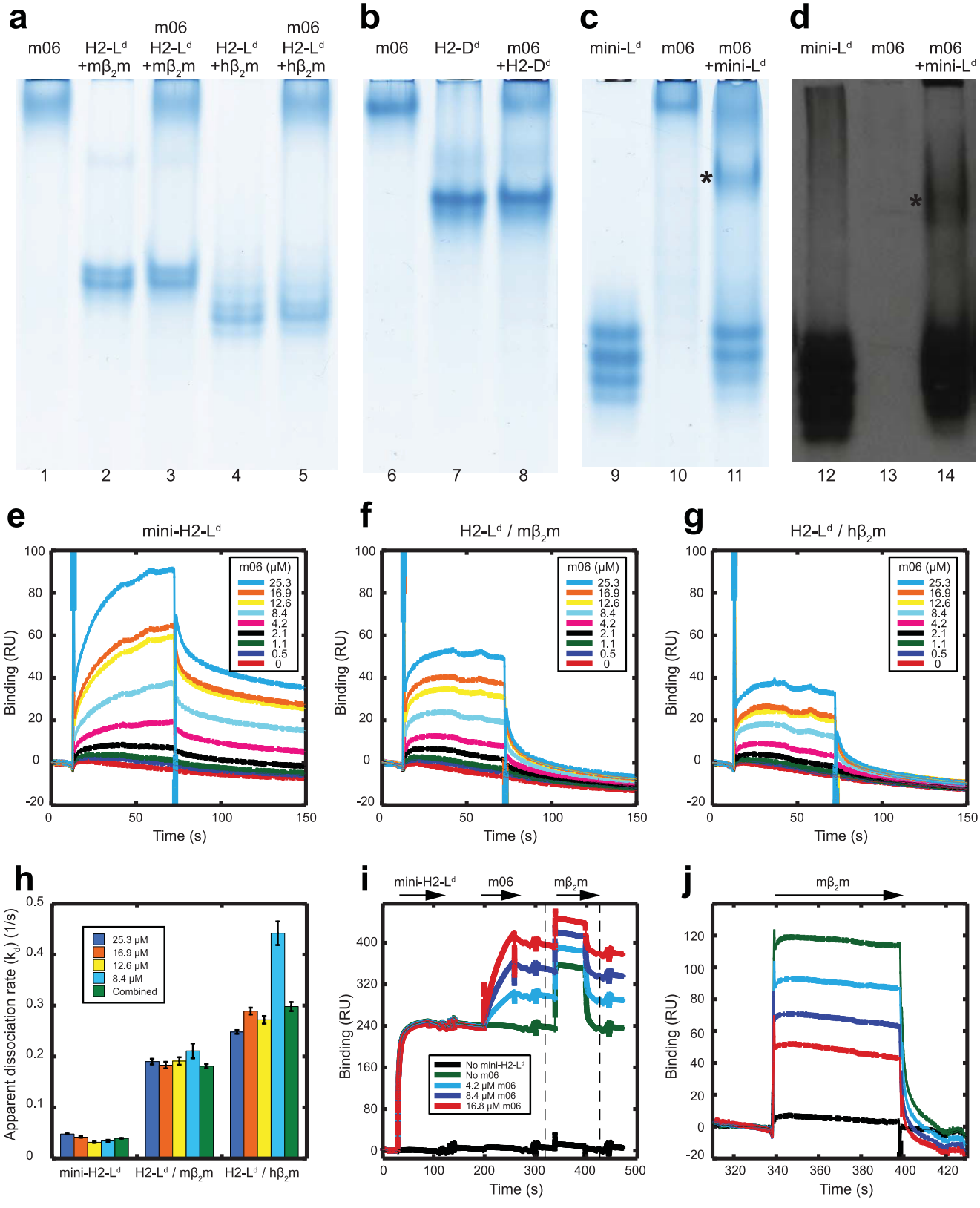

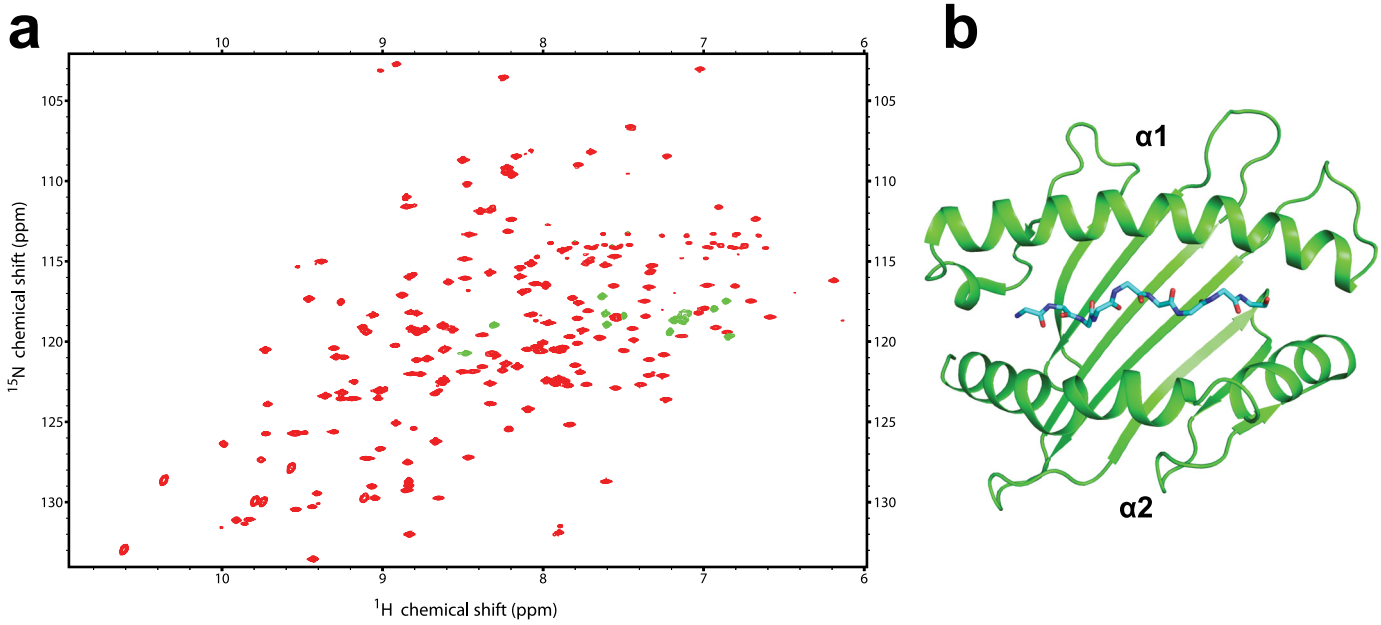

FIGURE 3. **NMR spectrum of the mini-H2-L^d·NIH peptide complex.** *a*, two-dimensional TROSY amide ^{1}H-^{15}N correlation spectrum of a 0.9 mM sample of mini-H2-L^d refolded *in vitro* with the peptide YPNVNIHNF. The sample shows exceptional stability, and the same spectrum can be obtained after several months of storage at 4 °C. Negative (*green*) peaks correspond to the Arg H$^\varepsilon$ protons that are folded in the ^{15}N dimension. *b*, structure diagram of the same protein construct extracted from the co-crystal structure of its complex with QL9 peptide and 2C T cell receptor (PDB entry 3TF7) (15). The peptide conformation is shown in a *stick representation*, backbone only.

surface coupled with 30-5-7S antibody to the α2 domain of H2-L^d, followed immediately by exposure to up to 25.3 μM m06 (Fig. 2, *e*–*g*). We found that m06 bound robustly to the 30-5-7S-captured mini-H2-L^d protein. However, m06 interacts only weakly with full-length H2-L^d·mβ_2m with a more rapid apparent dissociation rate (Fig. 2*f*). H2-L^d refolded with human β_2m showed detectable (within the limits of the method) but even weaker binding to m06 than the H2-L^d·mβ_2m complexes (Fig. 2*g*). The apparent dissociation rates, k_d, of the binding of m06 to mini-H2-L^d, H2-L^d·mβ_2m, and H2-L^d·hβ_2m, plotted in Fig. 2*h*, are consistent with the inability to detect complex formation of the full-length molecules in the gel shift assay. The continual dissociation of the captured H2-L^d protein from the antibody surface complicates quantitative analysis of the binding of m06 in this system, but consistently we observed strong binding by mini-H2-L^d and much attenuated binding in the case of H2-L^d·hβ_2m. The apparent ability of m06 to bind tightly to the mini-H2-L^d suggests that m06 may recognize a surface that is partially occluded on folded full-length, β_2m-associated MHC-I molecules.

To explore further the potential for competition between m06 and β_2m, we performed SPR experiments, first capturing mini-H2-L^d on a 30-5-7S surface, followed by exposure to m06, and then quickly shifting to a high, 1.2 mM concentration of murine β_2m (Fig. 2*i*). This concentration of β_2m resulted in clear association with the captured mini-H2-L^d but no nonspecific association with the antibody surface without captured mini-H2-L^d. When the captured mini-H2-L^d was first exposed to m06, the increase in binding (resonance units) during the β_2m binding step proportionately decreased, suggesting that m06 occupancy on mini-H2-L^d molecules prevents subsequent β_2m binding (Fig. 2, *i* and *j*). Finally, using NMR, we screened a sample containing 0.15 mM ^{13}C/^{15}N/^{2}H-labeled full-length H2-L^d MHC-I heavy chain, refolded with unlabeled human β_2m and NIH peptide, for binding to unlabeled m06 at a 1:1 molar ratio. The absence of any chemical shift changes or line broadening confirms that the K_d of the interaction between m06 and the full-length MHC is weaker than ~1 mM under the NMR conditions, consistent with a competition between β_2m and m06 for binding to a partially overlapping MHC-I epitope.

Peptide Optimization of Mini-H2-L^d Construct and NMR Backbone Assignments—Whereas a single MHC-I allele can generally refold using any of a number of peptides that satisfy a set of sequence rules imposed by the structure of the MHC-I-binding pockets (known as peptide "motifs" (40)), the stability of the resulting peptide·MHC-I complex is greatly influenced by the intrinsic affinity of the bound peptide because molecules that lose their peptides are prone to aggregation (41). NMR

FIGURE 2. **m06 associates tightly with mini-H2-L^d protein and weakly with full-length H2-L^d.** Native gel electrophoresis patterns of complexes between m06 and H2-L^d refolded with NIH peptide and either murine (final concentrations 13 μM m06 and 6 μM H2-L^d·mβ_2m) or human β_2m (12 μM m06, 4 μM H2-L^d·hβ_2m) (*a*); H2-D^d refolded with P18-I10 peptide and murine β_2m (24 μM m06, 19 μM H2-D^d) (*b*); and mini-H2-L^d refolded with NIH peptide (13 μM m06, 19 μM mini-H2-L^d) (*c*). *d*, complexes as shown in *c* were resolved by native gel electrophoresis and subsequently transferred to nitrocellulose membrane and probed for the presence of H2-L^d using the 64-3-7 mAb, which recognizes an epitope on the α1 domain of H2-L^d. Complexes between mini-H2-L^d and m06 in *c* and *d* are denoted with *asterisks*. *e*–*g*, a surface coupled to 30-5-7S antibody to H2-L^d α2 domain was used to capture H2-L^d to saturation levels prior to exposure to a range of m06 concentrations (0.5–25.3 μM, as indicated). *h*, apparent dissociation rates of m06 from H2-L^d constructs used in *e*–*g* are plotted for each of the four highest m06 concentrations used (8.4–25.3 μM, as indicated) as well as the composite of those concentrations. *Error bars*, S.E. *i*, a surface coupled to 30-5-7S antibody was used to capture mini-H2-L^d, followed by treatment with a range of m06 concentrations (0–16.8 μM, as indicated), followed by exposure to 1.2 mM mβ_2m. A control with no initial capture of mini-H2-L^d or m06 prior to mβ_2m exposure is shown in *black*. The *dashed lines* indicate the β_2m binding step, which is expanded in *j* and baseline-adjusted immediately prior to the exposure to mβ_2m. *RU*, resonance units.

allows the exploration of the conformational stability of MHC-I complexes with different bound peptides by monitoring the "fingerprint" features of two-dimensional amide ^{1}H-^{15}N correlation spectra over time. Toward this end, we prepared samples of the mini-H2-L^{d} construct refolded *in vitro* with two different peptides. In particular, we used the QL9 peptide (21) (also employed previously to study binding to the 2C TCR (13, 16, 17)) and a high affinity NIH self-peptide. Although initially, both samples gave well dispersed two-dimensional TROSY spectra, each indicative of a properly conformed peptide·MHC-I complex, the sample prepared with QL9 deteriorated within 1 week at 25 °C. This is consistent with the previous NMR study of the QL9 peptide·mini-H2-L^{d} complex, which reported transient self-association, leading to signal loss in the NMR experiments due to intermediate time scale conformational exchange with a high molecular weight form (13).

Notably, using the higher affinity NIH peptide, we were able to obtain stable samples of improved spectral quality and stability. We therefore prepared a 0.9 mM sample of $^{13}C/^{15}N/^{2}H$-labeled mini-H2-L^{d} folded with the NIH peptide (Fig. 3). Using this sample, we recorded a three-dimensional ^{15}N-separated amide NOESY spectrum in addition to a full array of triple resonance experiments (HNCO, HN(CA)CO, HNCA, and HN(CA)CB). From these complementary data sets, we obtained complete backbone assignments by mapping residue connectivity through the amide hydrogens, in addition to the backbone CO, Cα, and Cβ atoms (42). The improved stability and lack of aggregation were evident even after 2 weeks of data collection at 25 °C, where there was no loss of signal in two-dimensional TROSY-HSQC spectra. The spectral quality of mini-H2-L^{d} with NIH peptide enabled us to record RDCs under dilute alignment conditions using a Pf1 phage liquid crystalline sample (32) (as outlined in detail under "Experimental Procedures"). RDCs are sensitive probes of the local and long range structure that report on the relative orientation of backbone amide vectors along the protein sequence (43). Their quantitative comparison with the same parameters back-calculated from the x-ray coordinates of mini-H2-L^{d} confirms that the solution structure of our NMR construct is very similar to the crystal structure, with a *Q*-factor of 31%. Such a *Q*-factor is typical for the levels of structural noise present in x-ray structures (44). With this information at hand, we proceeded to examine the backbone dynamics of mini-H2-L^{d} in detail and to map the binding site for m06.

Backbone Dynamics of the Peptide·MHC-I Complex—The prolonged stability of the mini-H2-L^{d}·NIH peptide sample allowed us to perform a full suite of ^{15}N relaxation experiments (45) toward a characterization of backbone mobility. A quantitative assessment of MHC-I dynamics can help identify flexible and rigid regions that could serve as binding sites for immunoevasins and other cognate immune receptors. We recorded $R_{1\rho}$, heteronuclear NOE, and R_1 TROSY-based experiments (30) at 600 MHz, supplemented with R_1 measurements at 900 MHz. The extracted R_1 and R_2 relaxation rates together with the ^{15}N-$\{^{1}H\}$ NOE values are sensitive probes of the degree of motional restriction of the backbone amide N–H bond vectors on a time scale that is faster than the rotational diffusion of the molecule

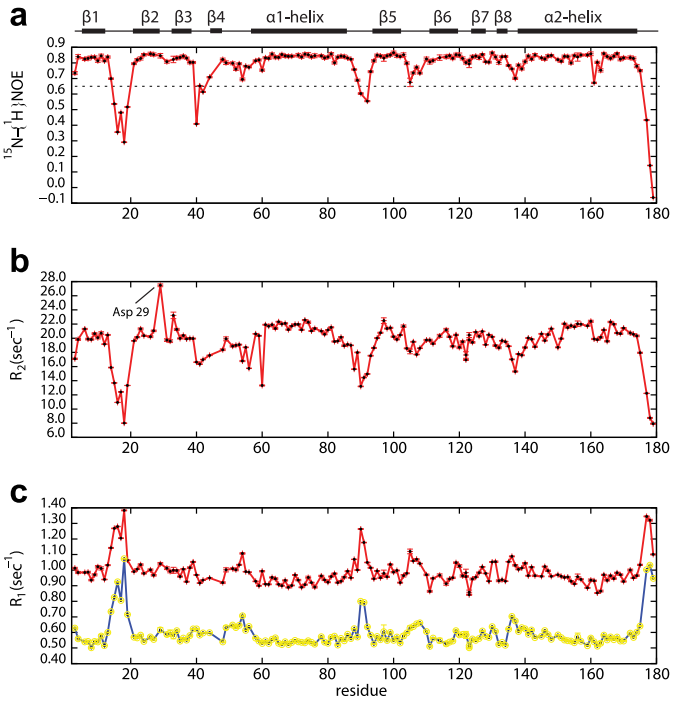

FIGURE 4. **^{15}N NMR relaxation data reporting on the backbone mobility of mini-H2-L^{d} for each residue, using the crystal structure (PDB entry 3TF7) as a reference.** *a*, ^{15}N-$\{^{1}H\}$ NOE values recorded at 600 MHz using TROSY-based methods. *b*, R_2 values (600 MHz), as obtained from measured $R_{1\rho}$ rates using a 2-kHz spin-lock field, after correction for off-resonance effects (31). *c*, longitudinal ^{15}N relaxation rates, R_1, (*red*, 600 MHz data; *yellow*, 900 MHz). All data were recorded using a 0.9 mM $^{15}N/^{2}H$-labeled sample of mini-H2-L^{d} in the NMR buffer (20 mM PIPES, pH 6.4, 50 mM NaCl) and are consistent with a predominantly monomeric form (70%) with a rotational correlation time of 13.2 ns/rad. The secondary structure diagram based on the DSSP annotation of the crystal structure is shown at the *top* as a guide.

(47), typically expressed by an exponential time constant τ_c (12–14 ns/rad for a 21-kDa protein at 25 °C). ^{15}N-$\{^{1}H\}$ NOE values are dominated by motions on the subnanosecond time scale, and values below 0.8 are indicative of such motions, with lower values corresponding to progressively larger amplitudes. These measurements are complemented by R_2 rates, with decreased values being indicative of internal dynamics of the amide N-H vector on a time scale faster than the molecular tumbling (~13 ns for mini-H2-L^{d}), whereas significantly elevated rates result from conformational exchange processes on a much slower time scale (>10 μs). Finally, R_1 rates probe motions at the angular ^{15}N frequencies (~3 ns for 600 MHz; ~2 ns for 900 MHz) and for a rigid backbone are dominated by the slow overall tumbling of the protein. Increases above the average value are indicative of internal motions and correlate with below average ^{15}N-$\{^{1}H\}$ NOE values.

Inspection of backbone relaxation rates of different amide sites along the MHC-I sequence (Fig. 4) shows several flexible regions of the molecule. In particular, loop residues 13–18 (β1–β2), 39–43 (β3–β4), and 87–92 (α1–β5), all located on the α1 half of the molecule, show ^{15}N-$\{^{1}H\}$ NOE and R_2 values that are much below average (~0.8 and 20 s^{-1}, respectively, in Fig. 4, *a* and *b*) and increased R_1 values (Fig. 4*c*), which are indicative of increased mobility on the picosecond-nanosecond time scale. The last four residues at the C terminus (not visible in the crystal structures) are also highly flexible. In addition, Asp-29

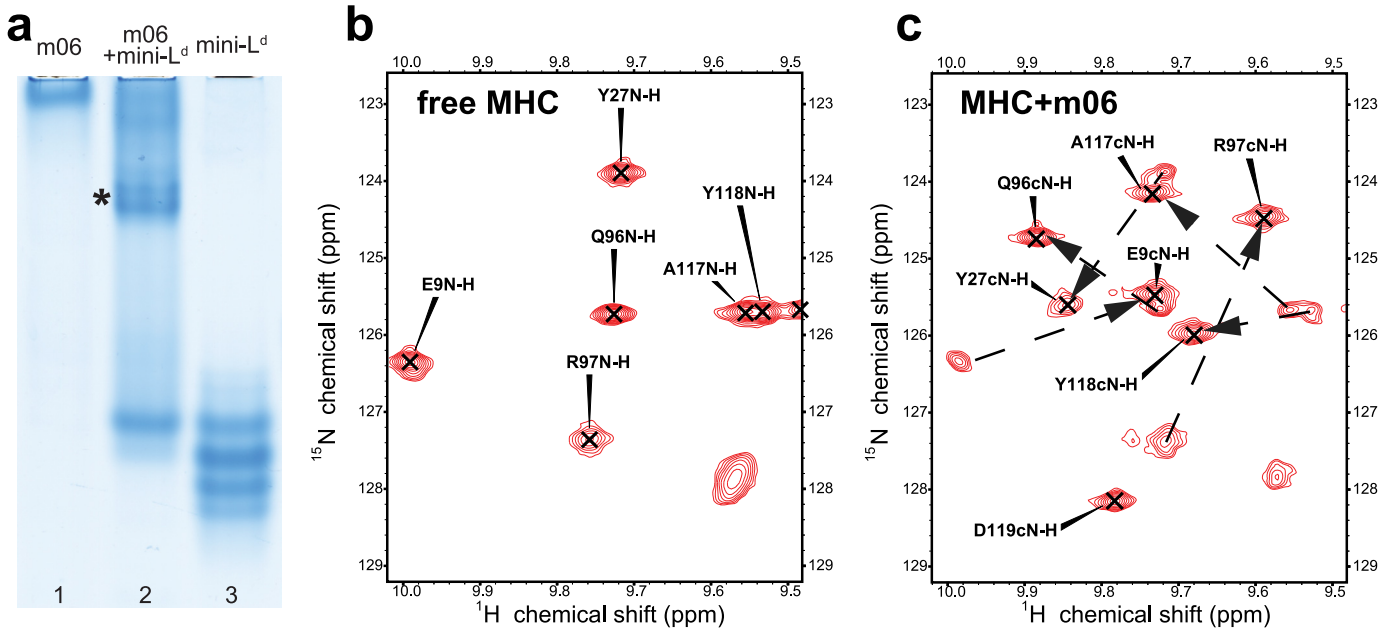

FIGURE 5. **m06 forms a tight complex with mini-H2-L^d in slow conformational exchange with the free form of mini-H2-L^d.** *a*, native gel shift assay showing the formation of a high affinity complex between m06 and mini-H2-L^d. *Lane 2* contains the m06/mini-H2-L^d mixture used in the NMR assays, diluted in native gel loading buffer to final concentrations of 32 μM m06 and 40 μM mini-H2-L^d. The m06·mini-H2-L^d complex is denoted with an *asterisk*. *b*, selected regions from TROSY-HSQC spectra of free mini-H2-L^d MHC-I; and *c*, a 1:0.8 mixture of mini-H2-L^d·m06 at pH 6.4 in 20 mM PIPES buffer, 50 mM NaCl, 25 °C, showing the formation of a tight complex between the two proteins in slow conformational exchange. The assignments of the free (*b*) and complex forms (*c*) are indicated for a single set of resonances in each spectrum.

located on the β_2-β_3 loop shows an increased R_2 rate, indicative of exchange between different conformations on the micro- to millisecond time scale. In contrast, the three shorter loops facing the α2 helix (residues 28–30, 104–108, and 126–133) appear well ordered according to the NMR relaxation data and are stabilized by a network of hydrogen bonds in the crystal structure of the molecule. The comparative rigidity of the α2 domain as a whole is consistent with the stabilization resulting from the conserved disulfide bond bridging the α2 helix with the β-sheet of all MHC-I molecules.

Identification of a Discrete Binding Site in Slow Conformational Exchange—To identify the binding site of m06 on MHC-I, we mixed unlabeled m06 with ^{13}C/^{15}N/^{2}H-labeled mini-H2-L^d at a ~0.8:1 molar ratio. As expected from the native gel shift results, m06 forms a tight complex with MHC-I under the NMR conditions, with nearly all MHC-I molecules in the bound state (Fig. 5*a*). The exchange between free and bound forms of MHC-I is slow on the NMR time scale, as indicated by the observation of a separate set of peaks for the complexed form (Fig. 5*c*). The rate of exchange between the free and bound forms was further investigated by NOE experiments and ZZ-exchange experiments with long mixing times relative to $1/R_1$ (48). However, these did not show any observable cross-peaks between the free and complex peaks, consistent with an upper limit for the dissociation constant in the low micromolar range, assuming a diffusion-limited on-rate. Because the resonances in the complex are shifted significantly in the ^{15}N, amide ^{1}H, and ^{13}CO dimensions, resonance assignment for the complexed form in crowded regions of the spectra is not straightforward (Fig. 5*b*). We therefore recorded optimized HNCA and HN(CA)CB spectra, in addition to a three-dimensional ^{15}N-separated amide NOESY spectrum. These spectra allowed us to unambiguously assign the peaks in the complex and identify the ^{15}N, amide ^{1}H, and ^{13}CO dimension chemical shift changes upon m06 binding to mini-H2-L^d. The combined changes, scaled relative to ^{1}H (Fig. 6*a*), reveal several sites along the MHC-I surface that are affected by m06 binding. The chemical shift changes, although spread out along the primary sequence, cluster in a contiguous region on the MHC-I structure that is underneath the α1α2 MHC-I platform, on the opposite face of the peptide-binding groove (Fig. 6*b*). The affected residues form a "wedge" on the surface of the MHC-I molecule, with the most strongly perturbed residues found in the β-strands at residues 95–99 and 115–125, forming a portion of the floor of the peptide-binding platform, as well as a region from residue 133 to 146, which forms part of the α2 helix. Notably, the association with m06 causes virtually no chemical shift changes in residues distant from the binding site, including all residues of the α1 and part of the α2 helix, which are responsible for retaining bound peptide (Fig. 6*b*). The absence of significant chemical shift changes in the α1 helix and most of the α2 helix indicates that binding of m06 does not lead to release of MHC-I-bound peptide. Formally, changes in chemical shift indicate perturbation of the magnetic environment of the affected atoms, which could result from a change in dynamics or from small changes in local electric fields caused by binding. Notably, the resonances of the shifted residues showed line widths that were very similar to sites not perturbed by binding, indicating the absence of substantial changes in backbone dynamics. The presence of a contiguous area of sites with substantially perturbed chemical shifts on the surface of the protein therefore can be safely interpreted as representing the m06 binding site (49).

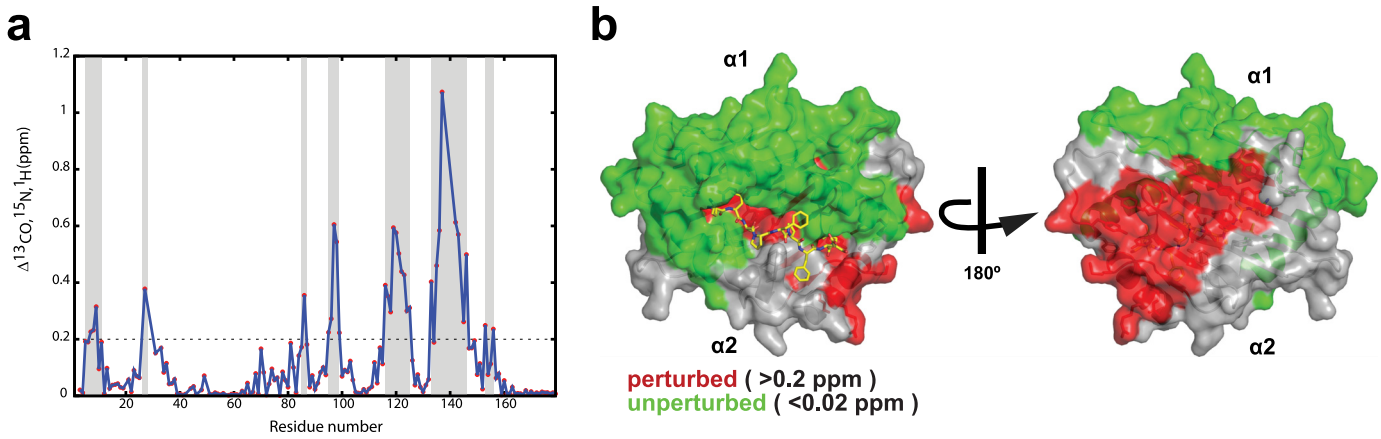

FIGURE 6. **Chemical shift mapping of the m06 interaction footprint on the x-ray structure of mini-H2-L^d.** *a* and *b*, combined backbone amide ^{1}H, ^{15}N, and ^{13}CO chemical shift differences (scaled relative to ^{1}H) for mini-H2-L^d are plotted (*a*) and illustrated (*b*) on the crystal structure of the same molecule (PDB entry 3TF7). Residues whose chemical shifts are significantly perturbed by m06 binding (chemical shift changes greater than 0.2 ppm) are shown in *red*, whereas sites whose chemical environment remains unaffected by m06 (shift changes less than 0.02 ppm) are in *green*. The remaining residues with perturbations between these thresholds are shown in *gray*. The assignments of the free and bound form are outlined under "Results," whereas examples of chemical shift perturbation results are shown in Fig. 5*c*.

Discussion

MHC-I interference by viral proteins is a multifaceted process involving the targeting of a number of distinct intermediates along the peptide loading and presentation pathway (1). For several proteins focused on the fully assembled MHC-I, the molecular mechanism of their interaction has been elucidated by x-ray crystallography of their MHC-I-bound complexes (50–52). Nevertheless, several stages of the MHC-I pathway have been resistant to crystallographic study, perhaps due to the dynamic nature of the complexes involved. Our results show an example in which high resolution NMR on a previously engineered minimal MHC-I construct is used to probe the dynamics of the free MHC-I construct and to characterize the complex form, revealing a novel m06 binding site on MHC-I, which is used by the virus to thwart the antigen presentation pathway inside the cell. These results demonstrate that the luminal domain of the MCMV m06/gp48 immunoevasin interacts only weakly with fully assembled MHC-I peptide·heavy chain·β_2m heterotrimers but binds with high affinity to mini-H2-L^d, which renders it amenable to detailed analysis by NMR.

The minimal MHC-I construct used in this study is an ideal model system to map the binding of cognate T cell receptors as well as viral molecules that may recognize the peptide-binding platform domain of the molecule. Sample optimization through careful selection of the MHC-I-bound peptide has enabled us to prepare labeled samples of prolonged stability and in milligram quantities typically required for NMR studies. The previous NMR characterization of the same construct lacked assignments of multiple amino acids under the $\alpha1\alpha2$ platform (13), and our assignments of those amino acids were instrumental in the precise mapping of the m06 binding site. The availability of a stable, fully assigned mini-H2-L^d construct enables an approach toward rapid and direct characterization of the binding sites for other putative MHC-I-associated proteins in a systematic manner using NMR spectroscopy.

During an MCMV infection, the m06 protein binds to and redirects full-length MHC-I molecules to lysosomes (5). Previous studies characterizing the interaction between m06 and MHC-I by pulse-labeling immunoprecipitation have shown that the β_2m subunit is part of the complex that is bound by m06 (3, 36). The ratio of recovered β_2m to heavy chain following m06 immunoprecipitation appears comparable with that observed in immunoprecipitations of properly folded, β_2m-associated heavy chain directly, suggesting that β_2m is an integral component of the MHC-I·m06 complex formed within the cell (3, 36). Despite this, we have only observed tight association between m06 and the mini-H2-L^d construct, whereas full-length MHC-I molecules (lacking the transmembrane domain) in association with β_2m bind m06 weakly *in vitro*. This difference in *in vitro* binding efficiency can be partially explained by the overlap between the observed binding site on the mini-H2-L^d protein and the binding site of β_2m on full-length MHC-I molecules, each on the underside of the MHC-I peptide binding platform (Fig. 7). Our β_2m competition experiments using SPR, in which binding of m06 to the mini-H2-L^d construct prevents subsequent β_2m association, further validate the NMR binding observation. We note that a crystal structure of the HLA-Aw68 $\alpha1\alpha2$ domain complexed with hβ_2m reveals that the interaction site of β_2m in the absence of the $\alpha3$ domain is the same as that of the intact heavy chain (53). This further supports the identification of the m06 footprint on MHC-I that we have determined here.

The overlap between the binding sites of m06 and β_2m raises the question of how the simultaneous interaction between m06, MHC-I heavy chain, and β_2m occurs within the cell. Notably, m06 recognizes an extensive surface on MHC-I, including part of the $\alpha2$ helix, thereby resulting in a much larger total footprint in the area under the $\alpha1\alpha2$ platform than β_2m. This surface also partially overlaps with the putative MHC-I binding site of the chaperone protein tapasin, which has been mapped by mutagenesis (54–56). m06 is expressed early during viral infection and first associates with MHC-I in the endoplasmic reticulum, the compartment where MHC-I folds and is assembled with β_2m and peptide (5). As a result, m06 might favorably compete with β_2m for the overlapping region on MHC-I, with the heavy chain using m06 as a scaffold for initial folding instead

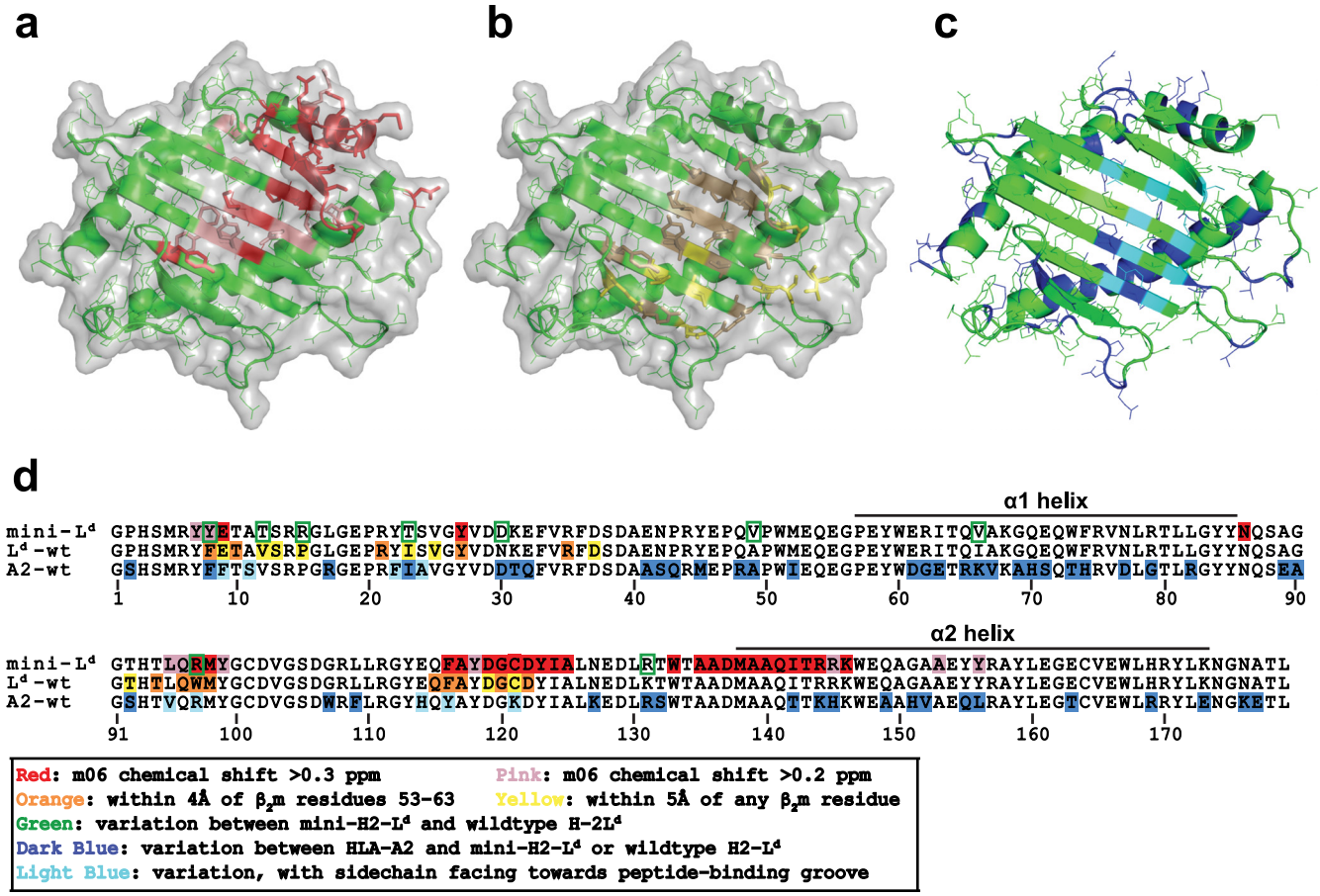

FIGURE 7. **Comparison of surfaces bound by m06 and β_2m and sequence alignment of H2-L^d with HLA-A2.** *Ribbon diagrams* in *a–c* are shown from the underside of the MHC-I peptide binding platform. *a*, residues experiencing a greater than 0.3-ppm chemical shift change upon m06 binding are shown in *red*, whereas residues with chemical shift changes between 0.2 and 0.3 ppm are shown in *pink*. *b*, residues of mini-H2-L^d that are within 4 Å of the residue 53–63 loop of β_2m as represented in the crystal structure of full-length H2-L^d (PDB entry 1LD9) are shown in *orange*, whereas additional residues within 5 Å of any β_2m residue are shown in *yellow*. *c*, residues of mini-H2-L^d that differ from those of HLA-A2 are shown in *dark blue* or in *light blue* if present on the floor of the β-sheet with side chains facing the interior of the molecule, oriented toward the peptide-binding groove. *d*, alignment of the $\alpha1\alpha2$ domains of mini-H2-L^d (*top*), wild type H2-L^d (*middle*), and HLA-A2 (*bottom*). Differences in amino acid sequence between minimal and wild type H2-L^d are indicated with *green boxes*. The sequences of minimal and wild type H2-L^d are annotated according to their contacts with m06 or β_2m, as in *a* and *b*. Amino acids that differ between HLA-A2 and either H2-L^d sequence are shown in *blue* or in *light blue* if the side chain of that residue is oriented toward the peptide-binding groove. *Ribbon diagrams* in *a–c* are taken from the crystal structure of mini-H2-L^d (PDB 3TF7).

of or in addition to β_2m (Fig. 8). Our *in vitro* binding assays require first preparing m06 and MHC-I separately, thus not enabling m06 to co-assemble with MHC-I molecules to form the three-component complex. Our SPR data support this model. In comparison with the mini-H2-L^d protein, properly conformed, full-length MHC-I shows reduced m06 binding *in vitro*. Furthermore, full-length H2-L^d in complex with human β_2m, which is well known to have a tighter association with heavy chain than murine β_2m (57–59), further limits m06 binding *in vitro*.

The characterization of the binding site by NMR and by SPR binding competition suggests that in order for m06 to co-assemble with MHC-I, the MHC-I/β_2m interface undergoes a local structural rearrangement. Knowledge of the dynamics of MHC-I heavy chain/β_2m interaction has largely been restricted to analysis of crystal structures, in which flexible regions of either protein are constrained in a single conformation. Recent studies of β_2m using NMR, both free in solution and in complex with MHC-I heavy chain, reveal a significant degree of flexibility in certain regions of β_2m (60, 61). In particular, the β-strand/loop composed of amino acids 53–63 of β_2m, which makes contact with the floor of the $\alpha1\alpha2$ platform of the heavy chain, is flexible in free β_2m and retains much of that flexibility upon association with heavy chain (61, 62). For example, the Lys-58 residue of human β_2m shifts by ~3.9 Å between its free and heavy chain-bound conformations and also shifts its conformation upon association with CD8$\alpha\alpha$ (62, 63). The flexible 53–63 loop of β_2m interacts with the $\alpha1\alpha2$ platform primarily in the same region bound by m06 (Fig. 7*b*). This observation suggests that the association between m06 and full-length, β_2m-bound heavy chain may involve a dislocation of this loop of the β_2m subunit, resulting in an alternate conformation of β_2m in complex with heavy chain and m06 in the context of an MCMV infection (Fig. 8). Alternatively, a contribution to the association by the transmembrane regions of the two molecules, not present in the constructs used here for the *in vitro* experiments, could explain the co-immunoprecipitation of m06 with MHC-I in the presence of β_2m.

The nucleotide sequences of many strains of MCMV have been determined, and their putative immunoevasion genes

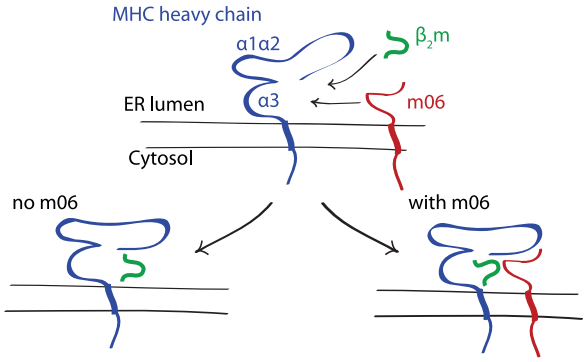

FIGURE 8. **Model for the co-assembly of MHC-I heavy chain, β_2m, and m06 in the cell.** MHC-I heavy chain is shown in *blue*, with the $\alpha1\alpha2$ and $\alpha3$ domains labeled. β_2m is shown in *green*, and m06 is shown in *red*. In the absence of m06, class I heavy chain associates normally with β_2m and peptide in the endoplasmic reticulum to form a properly conformed peptide·MHC-I complex for cell surface expression. m06 may exploit structural plasticity within the heavy chain/β_2m interface or interactions via the transmembrane domains, allowing co-assembly with the MHC and resulting in an altered association between β_2m and heavy chain.

have been examined (64, 65). In contrast to other members of the m02-16 family, which show high sequence divergence among MCMV strains, m06 sequences are extremely well conserved (65, 66). On the other hand, sequences of the structurally related m04 protein, also known to associate with MHC-I, are significantly variable among strains (64). In functional studies, m06 displays a broad specificity for murine MHC-I molecules (10). These observations, in combination with the strong sequence conservation of both the β_2m-binding surface and tapasin-binding regions of the class I heavy chain, help to explain both the evolutionary preservation of the sequence of m06 and its target specificity. To illustrate this, we aligned the sequences of the $\alpha1\alpha2$ domains of the mini-H2-L^d used in this study with those of wild-type H2-L^d as well as the more distantly related human HLA-A2 molecule (Fig. 7*d*). Due to constraints through their need to associate with β_2m, chaperone proteins like tapasin, and TCR and co-stimulatory molecules, the sequence variations among MHC-I alleles are primarily focused around the peptide-binding groove, whereas other surfaces are relatively conserved. The comparison of the sequence of the surface bound by the mini-H2-L^d and HLA-A2 illustrates this well; with only a few exceptions, all residues on the m06-binding surface of the mini-H2-L^d are identical in HLA-A2, or the variations in HLA-A2 are on the floor of the peptide-binding β-sheet with the altered side chain oriented toward the bound peptide rather than the exterior of the molecule (Fig. 7). This surface, conserved across MHC-I molecules by necessity, is exploited for binding by m06, enabling a broad target specificity for m06 (10). This strategy is a recurring theme in the recognition of MHC-I by viral immunoevasins, as exemplified here, and also in the co-crystal structures of MHC-I with other viral proteins (50–52).

Our identification of the m06 binding site on H2-L^d is a first step toward understanding the effects of m06 in the context of the broader immune evasion network of MCMV that includes the m04 and m152 viral proteins that modulate MHC-I. The luminal part of the m152 protein is believed to transiently associate with MHC-I (3) and has been crystallized in association with one of its target proteins, Rae1γ, which is bound across the top of the $\alpha1/\alpha2$ helices of the Rae1 MHC-I-like protein (67). Therefore, the interaction of m152 with MHC-I probably focuses on the opposite face of the peptide-binding platform relative to m06, consistent with the view that each protein binds a distinct site of MHC-I. Furthermore, despite m06 and m04 being closely related members of the same m02-m16 structural family, their behavior with regard to MHC-I binding may well be different. Whereas the luminal domain of m06 forms a tight complex with mini-H2-L^d (K_d in the low micromolar range by NMR, based on our observation of a tight complex with no detectable exchange), m04 shows only a weak affinity with H2-D^d MHC-I (K_d ~0.5–1 mM by SPR (11)). This result can be explained by the use of a full-length MHC-I molecule to probe m04 binding in our previous study and is in principle consistent with the binding site being partially occluded by β_2m in the fully assembled molecule. However, it has also been shown that the transmembrane domains of m04 and MHC-I contribute to their interaction (46), and the binding could thereby remain undetected in the recombinantly expressed luminal protein constructs used here and in previous m04 studies (11, 12). Post-translational modifications present in the naturally occurring molecules, not preserved in the bacterial molecules that we have studied, might also contribute to the interaction. The importance of the m04 transmembrane domain is further supported by the low sequence conservation of the m04 luminal domain among different viral isolates relative to m06 (64). The observation of a measurable interaction between m06 and MHC-I using just the luminal domains of the two molecules lacking the transmembrane domains suggests a distinct mode of engagement between m06 and m04. Taken together, these observations illustrate the diverse range of MHC-I binding sites and engagement strategies employed by MCMV to interfere with normal antigen processing of the cell, as exemplified by the m152, m06, and m04 paradigms.

Author Contributions—N. G. S., N. A. M., L. F. B., J. Y., A. B., and D. H. M. designed the experiments, executed experiments, and analyzed data. N. G. S., N. A. M., A. B., and D. H. M. wrote the paper.

Acknowledgments—We are indebted to Dr. David Kranz and Dr. Amy Hudson for providing the mini-H2-L^d- and m06-encoding plasmids, respectively, and to Dr. Kannan Natarajan for comments on the manuscript.

References

1. van de Weijer, M. L., Luteijn, R. D., and Wiertz, E. J. (2015) Viral immune evasion: lessons in MHC class I antigen presentation. *Semin. Immunol.* **27,** 125–137
2. Lemmermann, N. A., Fink, A., Podlech, J., Ebert, S., Wilhelmi, V., Böhm, V., Holtappels, R., and Reddehase, M. J. (2012) Murine cytomegalovirus immune evasion proteins operative in the MHC class I pathway of antigen processing and presentation: state of knowledge, revisions, and questions. *Med. Microbiol. Immunol.* **201,** 497–512
3. Ziegler, H., Muranyi, W., Burgert, H. G., Kremmer, E., and Koszinowski, U. H. (2000) The luminal part of the murine cytomegalovirus glycoprotein gp40 catalyzes the retention of MHC class I molecules. *EMBO J.* **19,** 870–881
4. Ziegler, H., Thale, R., Lucin, P., Muranyi, W., Flohr, T., Hengel, H., Farrell, H., Rawlinson, W., and Koszinowski, U. H. (1997) A mouse cytomegalo-

virus glycoprotein retains MHC class I complexes in the ERGIC/cis-Golgi compartments. *Immunity* **6,** 57–66
5. Reusch, U., Muranyi, W., Lucin, P., Burgert, H. G., Hengel, H., and Koszinowski, U. H. (1999) A cytomegalovirus glycoprotein re-routes MHC class I complexes to lysosomes for degradation. *EMBO J.* **18,** 1081–1091
6. Kleijnen, M. F., Huppa, J. B., Lucin, P., Mukherjee, S., Farrell, H., Campbell, A. E., Koszinowski, U. H., Hill, A. B., and Ploegh, H. L. (1997) A mouse cytomegalovirus glycoprotein, gp34, forms a complex with folded class I MHC molecules in the ER which is not retained but is transported to the cell surface. *EMBO J.* **16,** 685–694
7. Holtappels, R., Gillert-Marien, D., Thomas, D., Podlech, J., Deegen, P., Herter, S., Oehrlein-Karpi, S. A., Strand, D., Wagner, M., and Reddehase, M. J. (2006) Cytomegalovirus encodes a positive regulator of antigen presentation. *J. Virol.* **80,** 7613–7624
8. Babić, M., Pyzik, M., Zafirova, B., Mitrović, M., Butorac, V., Lanier, L. L., Krmpotić, A., Vidal, S. M., and Jonjić, S. (2010) Cytomegalovirus immunoevasin reveals the physiological role of "missing self" recognition in natural killer cell dependent virus control in vivo. *J. Exp. Med.* **207,** 2663–2673
9. Pinto, A. K., Munks, M. W., Koszinowski, U. H., and Hill, A. B. (2006) Coordinated function of murine cytomegalovirus genes completely inhibits CTL lysis. *J. Immunol.* **177,** 3225–3234
10. Wagner, M., Gutermann, A., Podlech, J., Reddehase, M. J., and Koszinowski, U. H. (2002) Major histocompatibility complex class I allele-specific cooperative and competitive interactions between immune evasion proteins of cytomegalovirus. *J. Exp. Med.* **196,** 805–816
11. Sgourakis, N. G., Natarajan, K., Ying, J., Vogeli, B., Boyd, L. F., Margulies, D. H., and Bax, A. (2014) The structure of mouse cytomegalovirus m04 protein obtained from sparse NMR data reveals a conserved fold of the m02-m06 viral immune modulator family. *Structure* **22,** 1263–1273
12. Berry, R., Vivian, J. P., Deuss, F. A., Balaji, G. R., Saunders, P. M., Lin, J., Littler, D. R., Brooks, A. G., and Rossjohn, J. (2014) The structure of the cytomegalovirus-encoded m04 glycoprotein, a prototypical member of the m02 family of immunoevasins. *J. Biol. Chem.* **289,** 23753–23763
13. Varani, L., Bankovich, A. J., Liu, C. W., Colf, L. A., Jones, L. L., Kranz, D. M., Puglisi, J. D., and Garcia, K. C. (2007) Solution mapping of T cell receptor docking footprints on peptide-MHC. *Proc. Natl. Acad. Sci. U.S.A.* **104,** 13080–13085
14. Jones, L. L., Brophy, S. E., Bankovich, A. J., Colf, L. A., Hanick, N. A., Garcia, K. C., and Kranz, D. M. (2006) Engineering and characterization of a stabilized α1/α2 module of the class I major histocompatibility complex product Ld. *J. Biol. Chem.* **281,** 25734–25744
15. Adams, J. J., Narayanan, S., Liu, B., Birnbaum, M. E., Kruse, A. C., Bowerman, N. A., Chen, W., Levin, A. M., Connolly, J. M., Zhu, C., Kranz, D. M., and Garcia, K. C. (2011) T cell receptor signaling is limited by docking geometry to peptide-major histocompatibility complex. *Immunity* **35,** 681–693
16. Hawse, W. F., De, S., Greenwood, A. I., Nicholson, L. K., Zajicek, J., Kovrigin, E. L., Kranz, D. M., Garcia, K. C., and Baker, B. M. (2014) TCR scanning of peptide/MHC through complementary matching of receptor and ligand molecular flexibility. *J. Immunol.* **192,** 2885–2891
17. Hawse, W. F., Champion, M. M., Joyce, M. V., Hellman, L. M., Hossain, M., Ryan, V., Pierce, B. G., Weng, Z., and Baker, B. M. (2012) Cutting edge: evidence for a dynamically driven T cell signaling mechanism. *J. Immunol.* **188,** 5819–5823
18. Kimpler, L. A., Glosson, N. L., Downs, D., Gonyo, P., May, N. A., and Hudson, A. W. (2014) Adaptor protein complexes AP-1 and AP-3 are required by the HHV-7 immunoevasin U21 for rerouting of class I MHC molecules to the lysosomal compartment. *PLoS One* **9,** e99139
19. Corr, M., Boyd, L. F., Frankel, S. R., Kozlowski, S., Padlan, E. A., and Margulies, D. H. (1992) Endogenous peptides of a soluble major histocompatibility complex class I molecule, H-2Lds: sequence motif, quantitative binding, and molecular modeling of the complex. *J. Exp. Med.* **176,** 1681–1692
20. Natarajan, K., Boyd, L. F., Schuck, P., Yokoyama, W. M., Eliat, D., and Margulies, D. H. (1999) Interaction of the NK cell inhibitory receptor Ly49A with H-2Dd: identification of a site distinct from the TCR site. *Immunity* **11,** 591–601
21. Chen, J., Eisen, H. N., and Kranz, D. M. (2003) A model T-cell receptor system for studying memory T-cell development. *Microbes Infect* **5,** 233–240
22. Ozato, K., Hansen, T. H., and Sachs, D. H. (1980) Monoclonal antibodies to mouse MHC antigens. II. Antibodies to the H-2Ld antigen, the products of a third polymorphic locus of the mouse major histocompatibility complex. *J. Immunol.* **125,** 2473–2477
23. Murre, C., Choi, E., Weis, J., Seidman, J. G., Ozato, K., Liu, L., Burakoff, S. J., and Reiss, C. S. (1984) Dissection of serological and cytolytic T lymphocyte epitopes on murine major histocompatibility antigens by a recombinant H-2 gene separating the first two external domains. *J. Exp. Med.* **160,** 167–178
24. Wang, R., Natarajan, K., Revilleza, M. J., Boyd, L. F., Zhi, L., Zhao, H., Robinson, H., and Margulies, D. H. (2012) Structural basis of mouse cytomegalovirus m152/gp40 interaction with RAE1γ reveals a paradigm for MHC/MHC interaction in immune evasion. *Proc. Natl. Acad. Sci. U.S.A.* **109,** E3578–E3587
25. Smith, J. D., Lie, W. R., Gorka, J., Kindle, C. S., Myers, N. B., and Hansen, T. H. (1992) Disparate interaction of peptide ligand with nascent versus mature class I major histocompatibility complex molecules: comparisons of peptide binding to alternative forms of Ld in cell lysates and the cell surface. *J. Exp. Med.* **175,** 191–202
26. Ying, J., Chill, J. H., Louis, J. M., and Bax, A. (2007) Mixed-time parallel evolution in multiple quantum NMR experiments: sensitivity and resolution enhancement in heteronuclear NMR. *J. Biomol. NMR* **37,** 195–204
27. Powers, R., Gronenborn, A. M., Clore, G. M., and Bax, A. (1991) 3-Dimensional triple-resonance NMR of C-13/N-15-enriched proteins using constant-time evolution. *J. Magn. Reson.* **94,** 209–213
28. Delaglio, F., Grzesiek, S., Vuister, G. W., Zhu, G., Pfeifer, J., and Bax, A. (1995) NMRPipe: a multidimensional spectral processing system based on UNIX pipes. *J. Biomol. NMR* **6,** 277–293
29. Goddard, T. D., and Kneller, D. G. (2008) *SPARKY3*, University of California, San Francisco
30. Lakomek, N. A., Ying, J., and Bax, A. (2012) Measurement of ^{15}N relaxation rates in perdeuterated proteins by TROSY-based methods. *J. Biomol. NMR* **53,** 209–221
31. Massi, F., Johnson, E., Wang, C., Rance, M., and Palmer, A. G., 3rd (2004) NMR R1 ρ rotating-frame relaxation with weak radio frequency fields. *J. Am. Chem. Soc.* **126,** 2247–2256
32. Zweckstetter, M., and Bax, A. (2001) Characterization of molecular alignment in aqueous suspensions of Pf1 bacteriophage. *J. Biomol. NMR* **20,** 365–377
33. Fitzkee, N. C., and Bax, A. (2010) Facile measurement of ^{1}H-^{15}N residual dipolar couplings in larger perdeuterated proteins. *J. Biomol. NMR* **48,** 65–70
34. Losonczi, J. A., Andrec, M., Fischer, M. W., and Prestegard, J. H. (1999) Order matrix analysis of residual dipolar couplings using singular value decomposition. *J. Magn. Reson.* **138,** 334–342
35. Rossi, P., Shi, L., Liu, G., Barbieri, C. M., Lee, H. W., Grant, T. D., Luft, J. R., Xiao, R., Acton, T. B., Snell, E. H., Montelione, G. T., Baker, D., Lange, O. F., and Sgourakis, N. G. (2015) A hybrid NMR/SAXS-based approach for discriminating oligomeric protein interfaces using Rosetta. *Proteins* **83,** 309–317
36. Bubeck, A., Reusch, U., Wagner, M., Ruppert, T., Muranyi, W., Kloetzel, P. M., and Koszinowski, U. H. (2002) The glycoprotein gp48 of murine cytomegalovirus: proteasome-dependent cytosolic dislocation and degradation. *J. Biol. Chem.* **277,** 2216–2224
37. Rammensee, H. G., Friede, T., and Stevanoviíc, S. (1995) MHC ligands and peptide motifs: first listing. *Immunogenetics* **41,** 178–228
38. Zhang, Y. (2008) I-TASSER server for protein 3D structure prediction. *BMC Bioinformatics* **9,** 40
39. Mage, M. G., Dolan, M. A., Wang, R., Boyd, L. F., Revilleza, M. J., Robinson, H., Natarajan, K., Myers, N. B., Hansen, T. H., and Margulies, D. H. (2012) The peptide-receptive transition state of MHC class I molecules: insight from structure and molecular dynamics. *J. Immunol.* **189,** 1391–1399
40. Falk, K., Rötzschke, O., Stevanović, S., Jung, G., and Rammensee, H. G. (1991) Allele-specific motifs revealed by sequencing of self-peptides eluted from MHC molecules. *Nature* **351,** 290–296

41. Bouvier, M., and Wiley, D. C. (1998) Structural characterization of a soluble and partially folded class I major histocompatibility heavy chain/β2m heterodimer. *Nat. Struct. Biol.* **5,** 377–384
42. Wuthrich, K. (1986) NMR of Proteins and Nucleic Acids, pp. 117–129, John Wiley & Sons, Inc., New York
43. Bax, A., and Grishaev, A. (2005) Weak alignment NMR: a hawk-eyed view of biomolecular structure. *Curr. Opin. Struct. Biol.* **15,** 563–570
44. Zweckstetter, M., and Bax, A. (2002) Evaluation of uncertainty in alignment tensors obtained from dipolar couplings. *J. Biomol. NMR* **23,** 127–137
45. Kay, L. E., Torchia, D. A., and Bax, A. (1989) Backbone dynamics of proteins as studied by N-15 inverse detected heteronuclear NMR-spectroscopy: application to staphylococcal nuclease. *Biochemistry* **28,** 8972–8979
46. Lu, X., Kavanagh, D. G., and Hill, A. B. (2006) Cellular and molecular requirements for association of the murine cytomegalovirus protein m4/gp34 with major histocompatibility complex class I molecules. *J. Virol.* **80,** 6048–6055
47. Lipari, G., and Szabo, A. (1982) Model-free approach to the interpretation of nuclear magnetic-resonance relaxation in macromolecules. 1. Theory and range of validity. *J. Am. Chem. Soc.* **104,** 4546–4559
48. Sahu, D., Clore, G. M., and Iwahara, J. (2007) TROSY-based z-exchange spectroscopy: application to the determination of the activation energy for intermolecular protein translocation between specific sites on different DNA molecules. *J. Am. Chem. Soc.* **129,** 13232–13237
49. Williamson, M. P. (2013) Using chemical shift perturbation to characterise ligand binding. *Prog. Nucl. Magn. Reson. Spectrosc.* **73,** 1–16
50. Gewurz, B. E., Wang, E. W., Tortorella, D., Schust, D. J., and Ploegh, H. L. (2001) Human cytomegalovirus US2 endoplasmic reticulum-lumenal domain dictates association with major histocompatibility complex class I in a locus-specific manner. *J. Virol.* **75,** 5197–5204
51. Li, L., Muzahim, Y., and Bouvier, M. (2012) Crystal structure of adenovirus E3–19K bound to HLA-A2 reveals mechanism for immunomodulation. *Nat. Struct. Mol. Biol.* **19,** 1176–1181
52. McCoy, W. H., 4th, Wang, X., Yokoyama, W. M., Hansen, T. H., and Fremont, D. H. (2013) Cowpox virus employs a two-pronged strategy to outflank MHCI antigen presentation. *Mol. Immunol.* **55,** 156–158
53. Collins, E. J., Garboczi, D. N., Karpusas, M. N., and Wiley, D. C. (1995) The three-dimensional structure of a class I major histocompatibility complex molecule missing the α3 domain of the heavy chain. *Proc. Natl. Acad. Sci. U.S.A.* **92,** 1218–1221
54. Peace-Brewer, A. L., Tussey, L. G., Matsui, M., Li, G., Quinn, D. G., and Frelinger, J. A. (1996) A point mutation in HLA-A*0201 results in failure to bind the TAP complex and to present virus-derived peptides to CTL. *Immunity* **4,** 505–514
55. Carreno, B. M., Solheim, J. C., Harris, M., Stroynowski, I., Connolly, J. M., and Hansen, T. H. (1995) TAP associates with a unique class I conformation, whereas calnexin associates with multiple class I forms in mouse and man. *J. Immunol.* **155,** 4726–4733
56. Yu, Y. Y., Turnquist, H. R., Myers, N. B., Balendiran, G. K., Hansen, T. H., and Solheim, J. C. (1999) An extensive region of an MHC class I α2 domain loop influences interaction with the assembly complex. *J. Immunol.* **163,** 4427–4433
57. Pedersen, L. O., Stryhn, A., Holter, T. L., Etzerodt, M., Gerwien, J., Nissen, M. H., Thøgersen, H. C., and Buus, S. (1995) The interaction of β2-microglobulin (β2m) with mouse class I major histocompatibility antigens and its ability to support peptide binding: a comparison of human and mouse β2m. *Eur. J. Immunol.* **25,** 1609–1616
58. Hebert, A. M., Strohmaier, J., Whitman, M. C., Chen, T., Gubina, E., Hill, D. M., Lewis, M. S., and Kozlowski, S. (2001) Kinetics and thermodynamics of β2-microglobulin binding to the α3 domain of major histocompatibility complex class I heavy chain. *Biochemistry* **40,** 5233–5242
59. Hochman, J. H., Shimizu, Y., DeMars, R., and Edidin, M. (1988) Specific associations of fluorescent β-2-microglobulin with cell surfaces: the affinity of different H-2 and HLA antigens for β-2-microglobulin. *J. Immunol.* **140,** 2322–2329
60. Beerbaum, M., Ballaschk, M., Erdmann, N., Schnick, C., Diehl, A., Uchanska-Ziegler, B., Ziegler, A., and Schmieder, P. (2013) NMR spectroscopy reveals unexpected structural variation at the protein-protein interface in MHC class I molecules. *J. Biomol. NMR* **57,** 167–178
61. Hee, C. S., Beerbaum, M., Loll, B., Ballaschk, M., Schmieder, P., Uchanska-Ziegler, B., and Ziegler, A. (2013) Dynamics of free *versus* complexed β_2-microglobulin and the evolution of interfaces in MHC class I molecules. *Immunogenetics* **65,** 157–172
62. Trinh, C. H., Smith, D. P., Kalverda, A. P., Phillips, S. E., and Radford, S. E. (2002) Crystal structure of monomeric human β-2-microglobulin reveals clues to its amyloidogenic properties. *Proc. Natl. Acad. Sci. U.S.A.* **99,** 9771–9776
63. Gao, G. F., Tormo, J., Gerth, U. C., Wyer, J. R., McMichael, A. J., Stuart, D. I., Bell, J. I., Jones, E. Y., and Jakobsen, B. K. (1997) Crystal structure of the complex between human CD8α(α) and HLA-A2. *Nature* **387,** 630–634
64. Smith, L. M., McWhorter, A. R., Shellam, G. R., and Redwood, A. J. (2013) The genome of murine cytomegalovirus is shaped by purifying selection and extensive recombination. *Virology* **435,** 258–268
65. Smith, L. M., Shellam, G. R., and Redwood, A. J. (2006) Genes of murine cytomegalovirus exist as a number of distinct genotypes. *Virology* **352,** 450–465
66. Corbett, A. J., Forbes, C. A., Moro, D., and Scalzo, A. A. (2007) Extensive sequence variation exists among isolates of murine cytomegalovirus within members of the m02 family of genes. *J. Gen. Virol.* **88,** 758–769
67. Wang, R., Natarajan, K., Revilleza, M. J. R., Boyd, L. F., Zhi, L., Zhao, H., Robinson, H., and Margulies, D. H. (2012) Structural basis of mouse cytomegalovirus m152/gp40 interaction with RAE1 γ reveals a paradigm for MHC/MHC interaction in immune evasion. *Proc. Natl. Acad. Sci. U.S.A.* **109,** E3578–E3587

A Novel MHC-I Surface Targeted for Binding by the MCMV m06 Immunoevasin Revealed by Solution NMR

Nikolaos G. Sgourakis, Nathan A. May, Lisa F. Boyd, Jinfa Ying, Ad Bax and David H. Margulies

J. Biol. Chem. 2015, 290:28857-28868.
doi: 10.1074/jbc.M115.689661 originally published online October 13, 2015
